Applied and Computational Mechanics 5 (2011) 205–216

Vibration of imperfect rotating disk

L. Půst[a,*], L. Pešek[a]

[a] *Institute of Thermomechanics AS CR, v. v. i., Dolejškova 5, 182 00 Praha 8, Czech Republic*

Received 2 October 2009; received in revised form 27 October 2011

Abstract

This study is concerned with the theoretical and numerical calculations of the flexural vibrations of a bladed disk. The main focus of this study is to elaborate the basic background for diagnostic and identification methods for ascertaining the main properties of the real structure or an experimental model of turbine disks. The reduction of undesirable vibrations of blades is proposed by using damping heads, which on the experimental model of turbine disk are applied only on a limited number of blades. This partial setting of damping heads introduces imperfection in mass, stiffness and damping distribution on the periphery and leads to more complicated dynamic properties than those of a perfect disk. Calculation of FEM model and analytic — numerical solution of disk behaviour in the limited (two modes) frequency range shows the splitting of resonance with an increasing speed of disk rotation. The spectrum of resonance is twice denser than that of a perfect disk.

Keywords: bladed disk, damping, imperfect disk, travelling waves

1. Introduction

The vibration of a turbine bladed disk is undesirable and highly dangerous, as it can lead to a failure by fatigue and may cause serious accidents. In order to quench these vibrations, various types of dampers are used. Even a small imperfection makes the vibration analysis more complicated. Large-scale research of these problems has been carried out in many institutes and laboratories in the world (e.g. [2–5, 9–11]). Experimental model investigated in the laboratories of the Institute of Thermomechanics (IT AS CR) consists of a steel disk with prismatic models of blades fastened on the perimeter of the disk. The disk is fixed in its centre either to the steel plate, or it is overhung on the rotating shaft. On the opposite ends of the disk's diameter, there are several blades equipped with damping heads.

2. FEM model

For a theoretical solution of deformations and stress, a three dimensional FE-model has been developed. The mesh structure is shown in Fig. 1. The eight-node hexagonal elements were used. Numerical method LANCZOS was applied for calculations of eigen-values and modes of vibrations. For modal analysis [6, 7], the damping elements were fixed to the ends of the blades.

Due to the added masses on the ends of selected blades, the bladed disk losses its perfect circular properties having infinite number of symmetry axes and therefore, becomes an imperfect disk with limited $2n$ number of axes. FEM solution enables to calculate all interested eigenfrequencies and modes of vibrations in very wide range of frequencies. This paper investigates the

*Corresponding author. Tel.: +420 266 053 212, e-mail: pust@it.cas.cz.

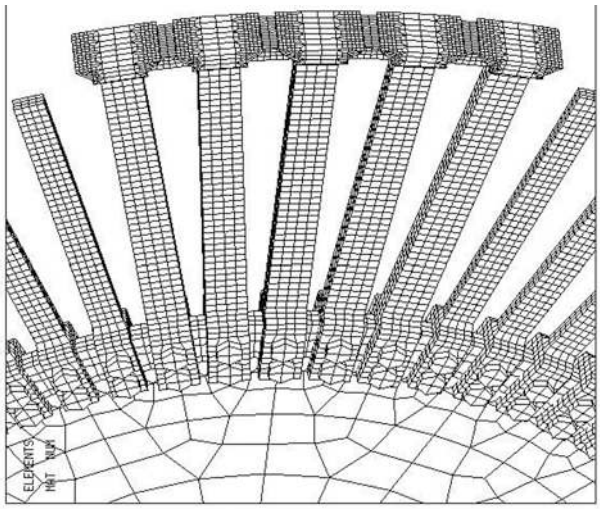

Fig. 1. Mesh structure of FE-model

eigenfrequencies of the two lowest modes of nodal diameters ($n = 1$ and $n = 2$) and no nodal circle ($l = 0$).

FEM calculated the lowest pairs of eigenfrequencies of a perfect, non-rotating bladed disk without any damping elements. The results are: $f_1 = 59.21$ Hz and $f_2 = 78.60$ Hz. Due to small masses added to the ends of five blades of selected groups, the bladed disk lost its perfect circular properties and became imperfect with a countable number of axes in this case two or four symmetry axes. The perfect disk has double eigenfrequencies f_1, f_2, which split into two pairs of close eigenfrequencies at the imperfect disks: $f_{1a} = 59.02$ Hz and $f_{1b} = 45.81$ Hz for $n = 1$ and $f_{2a} = 77.98$ Hz and $f_{2b} = 72.70$ Hz for $n = 2$.

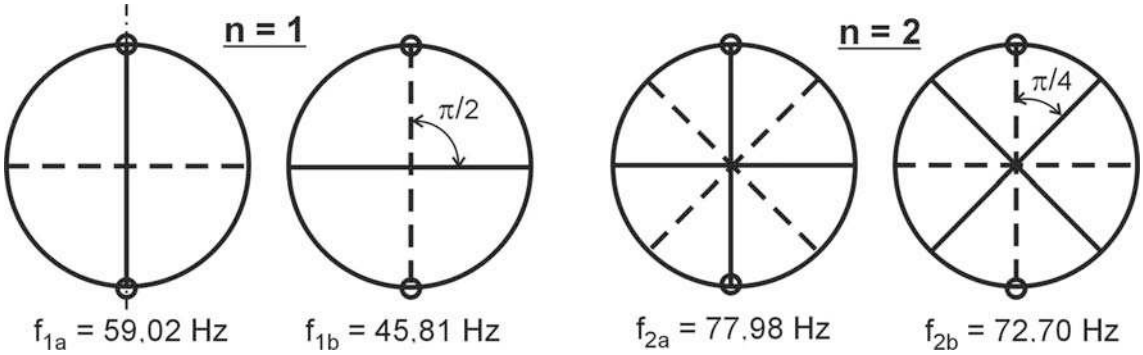

Fig. 2. Split modes with 1 and 2 nodal diameters

The imperfection of the bladed disk, caused by the addition of damper heads, results in free oscillations of two different orthogonal shape modes with the same number of nodal diameters, first ones (f_{1a}, f_{2a}) with one node line going through this imperfection (see full diameters in Fig. 2) and other ones (f_{1b}, f_{2b}) with this imperfection lying on one anti-node line (see dashed diameters in Fig. 2). For FEM modal analysis, the damping elements were stiff connected with the blade ends and created elastic shroud over five blades bundles. Therefore, no damping is present in the system calculated by FEM.

3. Experimental bladed disk model

The damping elements were attached to the real experimental bladed disk. These damping elements were formed as small masses among top-heads and were connected with them only by friction contacts. They allow the axial relative motion of heads, but suppress their relative turning and increase the bending stiffness, similar to the elastic shroud. Therefore these dampers are modelled for computation procedure not only by added masses Δm at the ends of the corresponding diameters, but also by increased damping Δb and stiffness Δc. These additional magnitudes must be multiplied twice, as there are two groups of damping heads.

3.1. Free vibrations of non-rotating disk

Free vibrations of the real experimental bladed disk can be investigated by means of four differential equations of the imperfect non-rotatig disk in the excitation frequency range ω near to the lowest eigenfrequencies f_1, f_2, i.e. approximately in $f \in (0, 100)$ Hz, or $\Omega = 2\pi f \in (0, 630)$ 1/s. These equations are in generalized coordinates q_{an}, q_{bn} $(n = 1, 2)$ as follows:

$$\begin{aligned} m_{redn}\ddot{q}_{an} + (b_{redn} + 2\Delta b)\dot{q}_{an} + c_{redn}q_{an} = 0, \\ (m_{redn} + 2\Delta m)\ddot{q}_{bn} + b_{redn}\dot{q}_{bn} + (c_{redn} + 2\Delta c)q_{bn} = 0, \qquad n = 1, 2, \end{aligned} \tag{1}$$

where m_{redn}, b_{redn}, c_{redn} are reduced values of perfect disk masses, damping and stiffness for the first $(n = 1)$ or second $(n = 2)$ mode of vibrations and are ascertained from the kinetic, potential energy and Rayleigh dissipative function of deformed bladed disk at corresponding modes [1, 8, 9].These values can be ascertained either from drawings by numerical calculation by means of some FE packages (e.g. ANSYS, CONSOL, etc.) or from data gained by measurements on a real structure or on its physical model.

Values q_{an}, q_{bn} are generalized coordinates belonging to the a – sine modes, b – cosine modes of stationary or rotating disk vibrations with n nodal diameters $n = 1$, $n = 2$, see Fig. 2. General coordinate system is connected and rotates together with the disk.

Additional damping $2\Delta b$ is added to the sine modes q_{an}, because this modes have the greatest shear deformations on the nodal diameter, i.e. in the damping heads position. Added mass and stiffness $2\Delta m$, $2\Delta c$ is zero in this position. On the contrary, the additional mass $2\Delta m$ and stiffness $2\Delta c$ strongly influence the vibrations of cosine modes q_{bn}, as they are in the anti-mode position.

3.2. Free un-damped vibrations

The various forms of vibrations of an un-damped disk $b_{red1} = b_{red2} = \Delta b = 0$, with amplitudes a_{na}, a_{nb} are described by

$$q_{an} = z_{na}(r, \phi) = a_{na} g_0(r) \sin n\phi, \qquad q_{bn} = z_{nb}(r, \phi) = a_{nb} g_0(r) \cos n\phi, \tag{2}$$

where φ is the circumferential angle, connection of radius r and rectangular coordinates x, y is $r = \sqrt{x^2 + y^2}$, $g_0(r)$ denotes the form of vibration in the radial direction; it depends on the structure and mass distribution of the disk vibrating with the mode of one or two nodal diameter and without any nodal circle. This function $g_0(r)$, which can be gained for given type of bladed disk either by FE solution, or by a measurement on real structures, is here supposed for simplicity to be equal for both $n = 1, 2$.

Indexes a, b ascertain the position of nodal diameters in relation to the position of the imperfection. Sinus forms correspond to the nodal diameters drawn by full lines at frequencies

f_{1a}, f_{2a}, in Fig. 2, cosine forms correspond to positions of nodal lines at frequencies f_{1b}, f_{2b}, in Fig. 2. The proper initial conditions in time $t = 0$ produce the general vibrations as combination of eigenmodes with common eigenfrequencies $\Omega_{na} = 2\pi f_{na}$, $\Omega_{nb} = 2\pi f_{nb}$ of the un-damped disk:

$$z(r,\phi,t) = \sum_{n=1}^{2} \left(a_{na} g_0(r) \sin n\phi \cos(\Omega_{na} t + \phi_{na}) + a_{nb} g_0(r) \cos n\phi \cos(\Omega_{nb} t + \phi_{nb})\right). \quad (3)$$

This expression contains eight free constants a_{1a}, ϕ_{1a}, a_{1b}, ϕ_{1b}, a_{2a}, ϕ_{2a}, a_{2b}, ϕ_{2b}, which can be determined by proper initial conditions. If the imperfection limits to zero, $\Omega_{na} \approx \Omega_{nb}$ and travelling waves which rotate on the disk by angular frequencies

$$\frac{\mathrm{d}\phi}{\mathrm{dt}} = \frac{\Omega_{nl}}{n} \qquad \text{or} \qquad \frac{\mathrm{d}\phi}{\mathrm{dt}} = -\frac{\Omega_{nl}}{n} \quad \text{for} \quad n = 1, 2 \quad (4)$$

can arise at appropriate initial conditions. However, damping in a real disk makes a quick decay of these free travelling wave oscillations.

The travelling waves exist in a non-rotating damped disk with imperfections when it is excited by a non-rotating harmonic force $F_0 \cos \omega t$ acting in a point between nodal (a) and anti-nodal (b) diameters as shown in Fig. 3. The strongest travelling waves appear if the frequency of exciting force lies in one of these intervals: $\omega \in (\Omega_{1a}, \Omega_{1b})$ or $\omega \in (\Omega_{2a}, \Omega_{2b})$ corresponding to the inter-resonance ranges. Differential equations of such system are derived in [6, 7, 9, 10] and are:

$$\begin{aligned} m_{redn}\ddot{q}_{an} + (b_{redn} + 2\Delta b)\dot{q}_{an} + c_{redn} q_{an} &= g_0(r_F), \sin n\phi F_0 \cos \omega t \sin n\lambda, \\ (m_{redn} + 2\Delta m)\ddot{q}_{bn} + b_{redn}\dot{q}_{bn} + (c_{redn} + 2\Delta c) q_{bn} &= g_0(r_F) \cos n\phi F_0 \cos \omega t \cos n\lambda, \\ & n = 1, 2. \end{aligned} \quad (5)$$

Here the left sides are identical with equations (1), q_n are generalized coordinates belonging to the eigen-forms at $n = 1$, $n = 2$. Radius r_F corresponds to the position of excitation force.

More detailed analysis of the stationary vibrations and travelling waves is presented in the publication [7].

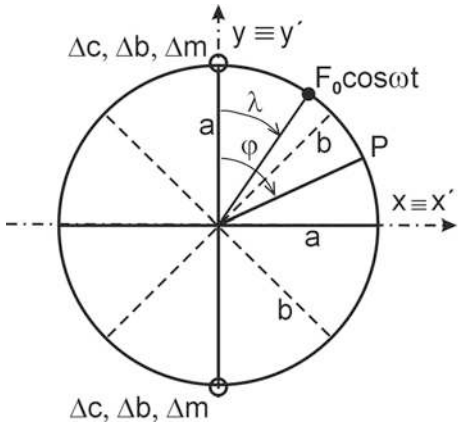

Fig. 3. Harmonic excitation of standing imperfect disk

4. Rotating imperfect disk

Dynamical properties of rotating imperfect disk with constant angular speed ν and modes of vibrations having n nodal diameters and no nodal circles are similar to those of stationary disk. However, one of the main differences observed are eigenfrequencies of the rotating disk which are increasing with increasing angular velocity ν:

$$\Omega_n = \Omega_{n,0} + c_n \nu^2.$$

Because revolutions of experimental equipment in IT ASCR are comparatively low, this change of frequency can be neglected in the following analysis.

Two coordinate systems are used to describe the investigated system:

1. A fixed one r, ϕ_a connected with the standing space,
2. Another coordinates r, ϕ connected to the rotating disk. Relation $\phi = \phi_a - \nu t$ is valid for the initial situation $\phi = \phi_a$ at $t = 0$.

Let in the fixed coordinate system 1) a harmonic force $F_0 \cos \omega t$ at $\phi_a = \lambda$ and at radius r_F near to the ends of blade acts on an imperfect disk, rotating with speed ν. In the disk coordinates 2), this force moves linearly with time in the negative direction ϕ and excites all modes of vibrations. Point of action of $F_0 \cos \omega t$ is given in rotating coordinates x', y' (see Fig. 4) by angle $\phi_F = \lambda - \nu t$, and a general point P of the disk has in the non-rotating coordinates increasing angle position $\phi_a = \phi + \nu t$. Vibrations of the rotating imperfect disk with one or two nodal diameters ($n = 1, 2$) are described by equations

$$\begin{gathered} m_{redn}\ddot{q}_{an} + (b_{redn} + 2\Delta b)\dot{q}_{an} + c_{redn} q_{an} = g_0(r_F) \sin n\phi F_0 \cos \omega t \sin n(\lambda - \nu t), \\ (m_{redn} + 2\Delta m)\ddot{q}_{bn} + b_{redn} dot q_{bn} + (c_{redn} + 2\Delta c) q_{bn} = g_0(r_F) \cos n\phi F_0 \cos \omega t \cos n(\lambda - \nu t), \\ n = 1, 2. \end{gathered} \tag{6}$$

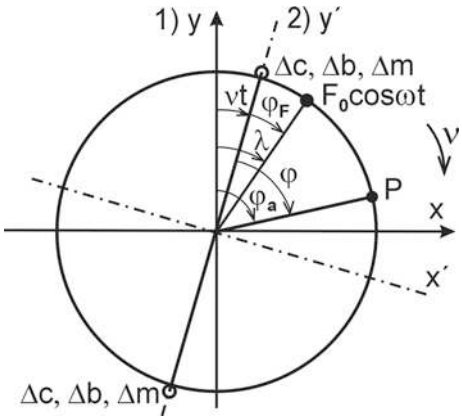

Fig. 4. Harmonic excitation of rotating imperfect disk

Simple arrangement of equations (6) by introducing expressions

$$u_{an} = \frac{q_{an} m_{redn}}{g_0(r_F) F_0}, \qquad u_{bn} = \frac{q_{bn}, m_{redn}}{g_0(r_F) F_0}, \qquad \Omega_{an}^2 = \frac{c_{redn}}{m_{redn}}, \qquad \Omega_{bn}^2 = \frac{c_{redn} + 2\Delta c_b}{m_{redn} + 2\Delta m},$$

$$\beta_{an} = \frac{b_{redn} + 2\Delta b}{m_{redn}}, \qquad \beta_{bn} = \frac{b_{redn}}{m_{redn} + 2\Delta m}, \qquad n = 1, 2 \tag{7}$$

gets equations

$$\begin{aligned} \ddot{u}_{an} + \beta_{an}\dot{u}_{an} + \Omega_{an}^2 u_{an} &= \cos\omega t \sin n\phi \sin n\nu t, \\ \ddot{u}_{bn} + \beta_{bn}\dot{u}_{bn} + \Omega_{bn}^2 u_{bn} &= \cos\omega t \cos n\phi \cos n\nu t, \end{aligned} \qquad n = 1, 2. \tag{8}$$

The dynamical parameters $\Omega_{an}, \Omega_{bn}, \ldots$ etc. of bladed disk can be ascertained either from working drawings by numerical calculation using some professional FE packages (e.g. ANSYS, COMSOL, etc.) or by measurements on a real structure or on its physical model. Values used in examples in this article are based on data gained from experiments carried out on simplified model of bladed disk in Dynamical Laboratory of Institute of Thermomechanics, ASCR.

The functions on the right sides of equations (8) are complicated functions of time — product of two harmonic functions. For a simple solution of forced vibrations it is convenient to transform these expressions into a sum of terms containing no more than one harmonic function of time:

$$\begin{aligned} \cos\omega t \sin n\nu t &= \left[\sin(\omega + n\nu)t - \sin(\omega - n\nu)t\right]/2, \\ \cos\omega t \cos n\nu t &= \left[\cos(\omega + n\nu)t + \cos(\omega - n\nu)t\right]/2, \end{aligned} \qquad n = 1, 2. \tag{9}$$

It is shown that one in space-fixed harmonic force $F_0 \cos\omega t$ acts on the rotating disk as two harmonic forces with different frequencies $(\omega + n\nu)$ and $(\omega - n\nu)$. These force-decompositions at appropriate values ω and ν cause travelling waves. Results of our analysis show that the response curves of a disk rotating at constant speed ν can have twice as many resonance peaks as the non-rotating disk.

Solution (8) after introduction (5) gives

$$\begin{aligned} u_{an} &= \frac{\sin n\phi \sin\left[(\omega + n\nu)t - \psi_{an1}\right]}{2\sqrt{(\Omega_{an}^2 - (\omega + n\nu)^2)^2 + \beta_{an}^2(\omega + n\nu)^2}} + \frac{\sin n\phi \sin\left[(\omega - n\nu)t - \psi_{an2}\right]}{2\sqrt{(\Omega_{an}^2 - (\omega - n\nu)^2)^2 + \beta_{an}^2(\omega - n\nu)^2}}, \\ u_{bn} &= \frac{\cos n\phi \cos\left[(\omega + n\nu)t - \psi_{bn1}\right]}{2\sqrt{(\Omega_{bn}^2 - (\omega + n\nu)^2)^2 + \beta_{bn}^2(\omega + n\nu)^2}} + \frac{\cos n\phi \cos\left[(\omega - n\nu)t - \psi_{bn2}\right]}{2\sqrt{(\Omega_{bn}^2 - (\omega - n\nu)^2)^2 + \beta_{bn}^2(\omega - 2\nu)^2}}, \\ & \qquad n = 1, 2. \end{aligned} \tag{10}$$

The corresponding phase angles are

$$\begin{aligned} \psi_{an1} &= \operatorname{arctg}\frac{\beta_{an}(\omega + n\nu)}{\Omega_{an}^2 - (\omega + n\nu)^2}, & \psi_{bn1} &= \operatorname{arctg}\frac{\beta_{bn}(\omega + n\nu)}{\Omega_{bn}^2 - (\omega + n\nu)^2}, \\ \psi_{an2} &= \operatorname{arctg}\frac{\beta_{an}(\omega - n\nu)}{\Omega_{an}^2 - (\omega - n\nu)^2}, & \psi_{bn2} &= \operatorname{arctg}\frac{\beta_{bn}(\omega - n\nu)}{\Omega_{bn}^2 - (\omega - n\nu)^2}, \end{aligned} \qquad n = 1, 2. \tag{11}$$

Dynamical coefficients in expressions (10)

$$\begin{aligned} &\frac{1}{\sqrt{(\Omega_{an}^2 - (\omega + n\nu)^2)^2 + \beta_{an}^2(\omega + n\nu)^2}}, & &\frac{1}{\sqrt{(\Omega_{an}^2 - (\omega - n\nu)^2)^2 + \beta_{an}^2(\omega - n\nu)^2}}, \\ &\frac{1}{\sqrt{(\Omega_{bn}^2 - (\omega + n\nu)^2)^2 + \beta_{bn}^2(\omega + n\nu)^2}}, & &\frac{1}{\sqrt{(\Omega_{bn}^2 - (\omega - n\nu)^2)^2 + \beta_{bn}^2(\omega - 2\nu)^2}} \end{aligned} \tag{12}$$

reach their maximum values at excitation frequencies

$$\begin{aligned} &\omega = \Omega_{a1} + \nu, \quad \omega = \Omega_{a1} - \nu, \quad \omega = \Omega_{b1} + \nu, \quad \omega = \Omega_{b1} - \nu, \\ &\omega = \Omega_{a2} + 2\nu, \quad \omega = \Omega_{a2} - 2\nu, \quad \omega = \Omega_{b2} + 2\nu, \quad \omega = \Omega_{b2} - 2\nu, \end{aligned} \tag{13}$$

at which the resonance peaks in response curves occur.

5. Response curves of rotating imperfect disk

The graphical representation of these properties for the first mode with one nodal diameter ($n = 1, l = 0$) is shown in Fig. 5 in the form of frequency-speed diagram [9].

The response curve of a stationary disk (disk speed $v = 0$) has two resonance peaks at $\omega = \Omega_{b1}$ and $\omega = \Omega_{a1}$, determined by the intersections of a vertical line A with the oblique thick lines. The thick lines correspond to equations in the first row (13). The response curve is drawn in Fig. 6.

Rotation at low revolutions, as observed in Fig. 5 line B at 200 rpm, causes that the two resonance peaks split into four, as seen in Fig. 7. The split resonances have lower height (ap-

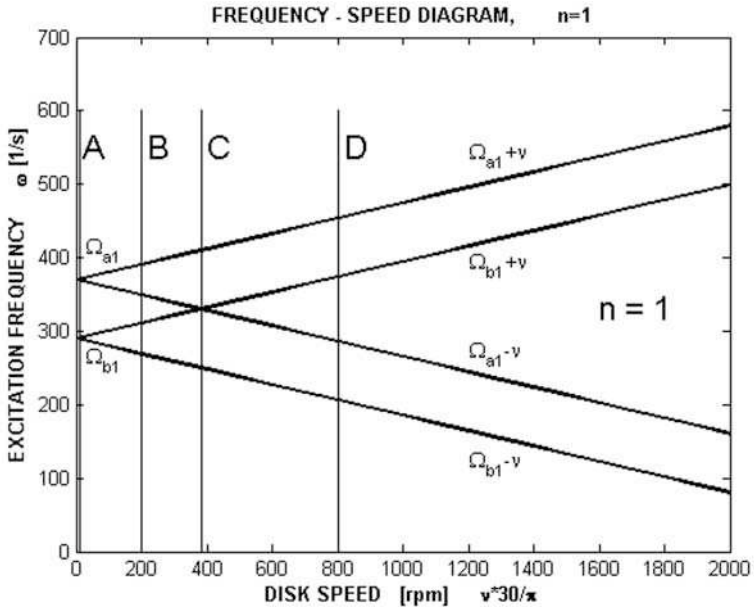

Fig. 5. Frequency-speed diagram of imperfect disk

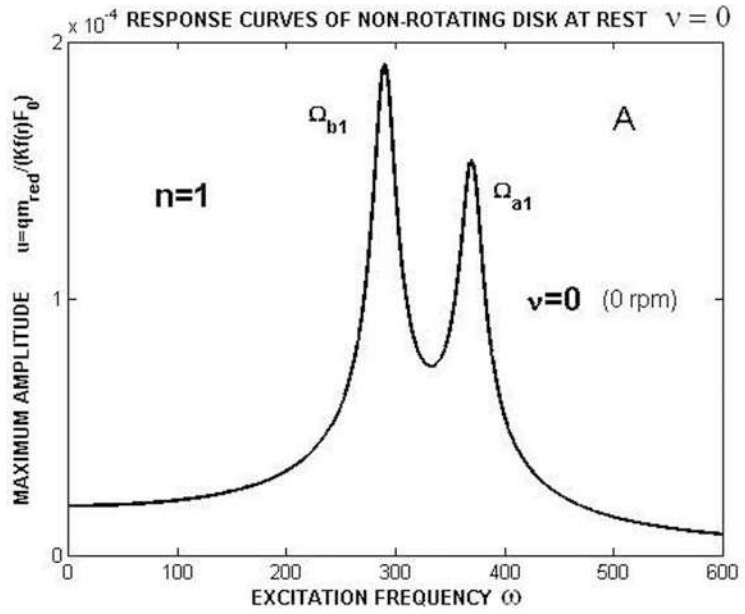

Fig. 6. Response curve of standing imperfect disk

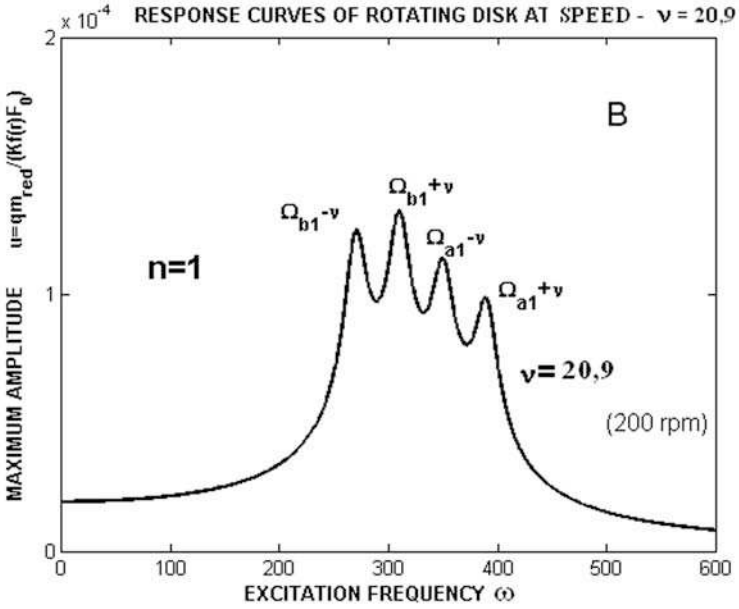

Fig. 7. Response curve of rotating (200 rpm) imperfect disk

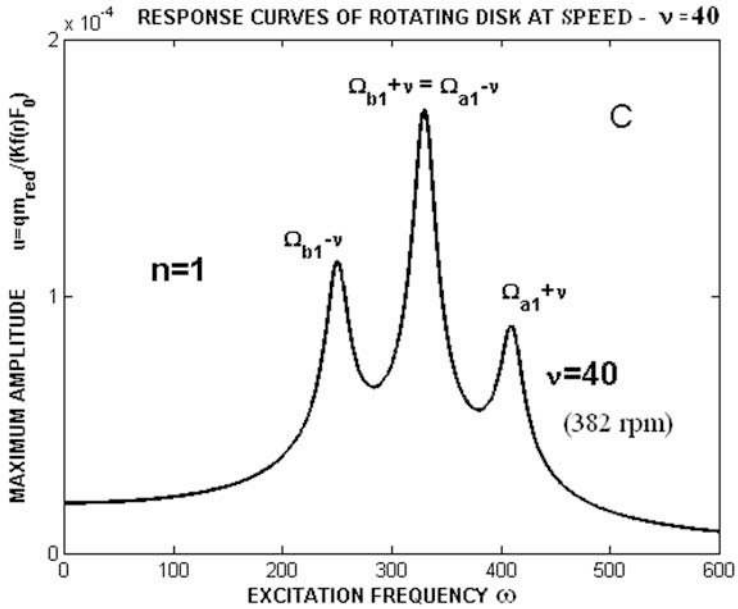

Fig. 8. Response curve of rotating (382 rpm) imperfect disk

proximately half) then those in Fig. 6. In both figures are dimension u [s^2] and ω [rad/s]. The same dimensions are used in Fig. 8, 9, 11, 12.

Line C in Fig. 5 at $\nu = 40$ rad/s goes through the point of intersection of lines given by equations $\omega = \Omega_{a1} - \nu$ and $\omega = \Omega_{b1} + \nu$.

Response curve of this case (shown in Fig. 8) has only three peaks. The combined resonance is higher then the neighbouring peaks at $\omega = \Omega_{b1} - \nu$ and $\omega = \Omega_{a1} + \nu$.

At a higher disk speed up to 800 rpm ($\nu = 83.81$ rad/s), represented by the line D in Fig. 5, the number of interactions increased to four again. Corresponding response curve is shown in Fig. 9. It is similar to Fig. 7 (200 rpm) except that the sequences of resonance peaks are different; the peaks with the mode b alter with a at increasing frequency of excitation ω.

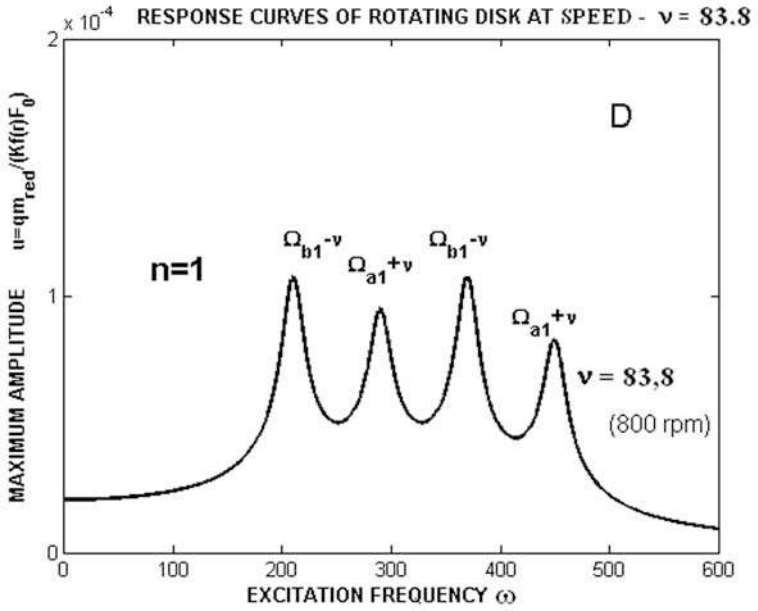

Fig. 9. Response curve of rotating (800 rpm) imperfect disk

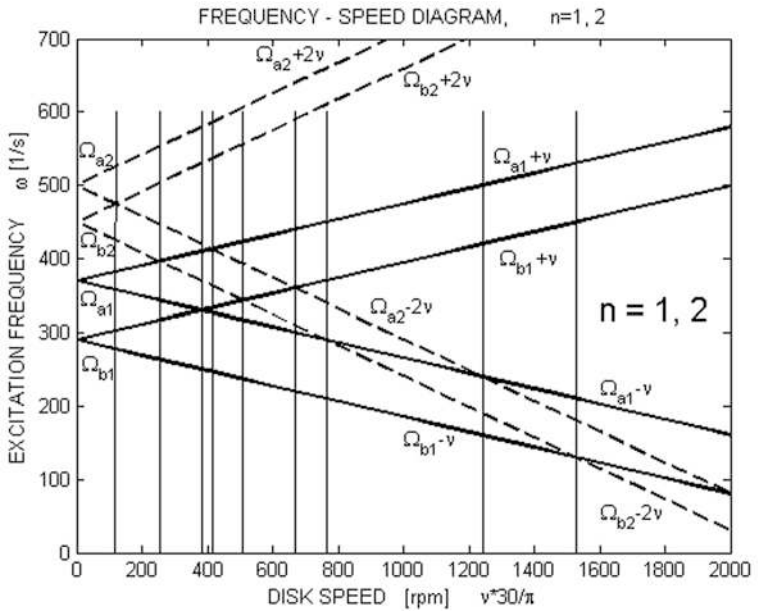

Fig. 10. Frequency-speed diagram of two lowest modes of imperfect disk

Results based on the analysis of disk vibrations when considering only one isolated mode ($n = 1$) cannot describe the full dynamic behaviour of the real rotating imperfect disk as it presents the rich spectrum of modes with various nodal diameters and nodal circles.

As an example of the increasing complications due to mutual interactions of disk modes with different number n of circumferential waves Fig. 10 shows frequency-speed diagram of rotating imperfect disk, where two basic modes $n = 1$ and $n = 2$ are considered. The thick full inclined lines correspond to the equations in the first row of (13) and illustrate the dynamic behaviour of $n = 1$ mode of disk vibrations. The thick dashed inclined lines belong to the second row of equations (13) and graphically demonstrate the dynamical properties of $n = 2$ mode of vibrations. Due to different gradient of lines for $n = 1$ and $n = 2$, ten points of

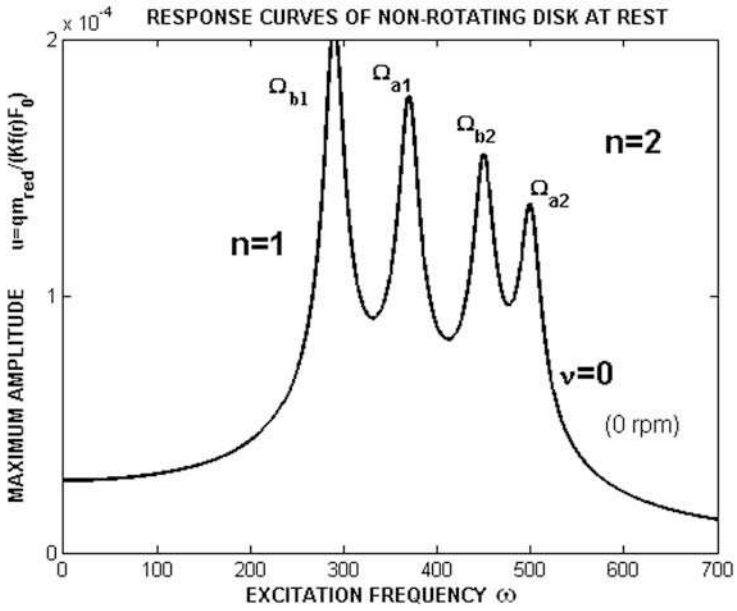

Fig. 11. Four resonance peaks of standing imperfect disk

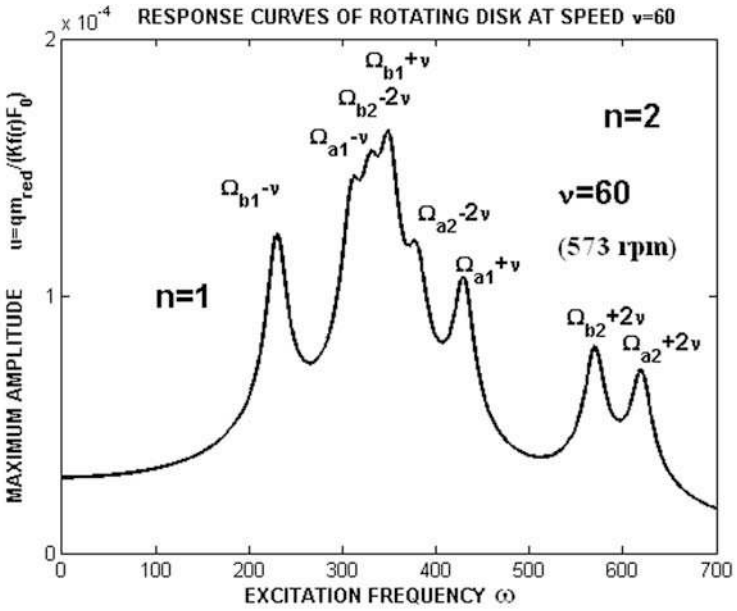

Fig. 12. Eight resonance peaks of rotating (573 rpm) imperfect disk

interaction are present in this diagram. They are marked by vertical lines, which, in general, intersect the thick inclined lines in points, giving the positions of resonance peaks of response curves.

The simplest response curve belonging to the standing non-rotating disk ($\upsilon = 0$) is shown in Fig. 11. There are four resonance peaks at $\omega = \Omega_{b1}; \Omega_{a1}; \Omega_{b2}; \Omega_{a2}$.

Rotation of disk ($\upsilon > 0$) causes the split of resonances again. Example of such response curve is shown in Fig. 12 for $\upsilon = 60$ rad/s. There are eight resonance peaks, but four of them are very close and form in the range $\omega \in (300, 400)$ rad/s a strong common resonance peak with four local peaks.

Similar, but in sequence of modes very different response curves are obtained at various speeds of a disk rotation. It is evident that the analysis of experimentally gained resonance curves of a rotating imperfect disk is extremely difficult without any detailed theoretical investigation.

6. Conclusion

This paper presents computational methods for the analysis of dynamic properties of a non-rotating or rotating disk. The circular disk fixed in its centre has many double eigenfrequencies, each one described by different numbers of nodal diameters and of nodal circles. Positions of nodal diameters are arbitrary at perfect disks, but they are fixed with respect to the position of imperfection at imperfect disks.

Investigated imperfection was formed by the attachment of two groups of vibration-damping heads on simplified model of an experimental bladed disk. Detail analysis was focused on the modes with one and two modal diameters and on the frequency range containing corresponding split resonance peaks. Analysis of dynamic properties of a rotating imperfect disk excited by an external single in space-fixed harmonic transversal force $F_0 \cos \omega t$ shows the existence of travelling waves, and split of eigenfrequencies depending on the rotation speed.

The response curves of the imperfect disk rotating with speed ν have twice as many resonance peaks than the same non-rotating disk.

This study is a contribution to the theoretical support of experimental research of a rotating model of a bladed disk carried out in Institute of Thermomechanics AS CR with the aim to investigate the influence of elastic, mass and damping imperfections on the dynamic behavior of turbine disks.

Acknowledgements

This work has been supported by the grant project GA CR 101/09/1166 “Research of dynamic behaviour and optimisation of complex rotating system with non-linear couplings and high damping materials”.

References

[1] Brepta, R., Půst, L., Turek, F., Mechanical vibrations, Technical guide No. 71, Sobotáles, Praha, 1994. (in Czech)

[2] Bucher, I., Feldman, M., Minikes, A., Gabay, R., Real-time travelling waves and whirl decomposition, Proceedings of the 8$^{\text{th}}$ International Conference on Vibrations in Rotating Machinery), IMechE 2004, Wiltshire, 2004, pp. 261–267.

[3] Pešek, L., et al., Dynamics of rotating blade disk identifical by magneto-kinematic measuring system, Proceedings of ISMA 2008, Leuven, Belgium, 2008, pp. 1 097–1 111.

[4] Půst, L., Applied continuum mechanics II: Continuum dynamics, ČVUT-FJFI, Praha, 1986. (in Czech)

[5] Půst, L., Effect of imperfection of rotary bodies on their vibrations, Proceedings of the V. National Congress on Theoretical and Aplied Mechanics, Vol. 3, Sofia, Bulgaria, 1985, pp. 131–136. (in Russian)

[6] Půst, L., Pešek, L., Traveling waves in circular disk with imperfections, Proceedings of the 10th Conference on Dynamical Systems – Theory and Applications, Vol. 1, Lodž, Poland, 2009, pp. 345–352.

[7] Půst, L., Pešek, L., Traveling waves in rotational machines, Proceedings of the conference Engineering Mechanics 2009, Svratka, Czech Republic, 2009, pp. 1 065–1 078.

[8] Slavík, J., Stejskal, V., Zeman, V., Basics of machine dynamics, ČVUT, Praha, 1997. (in Czech)

[9] Tobias, S. A., Arnold, R. N., The Influence of dynamical imperfection on the vibration of rotating disks, Proceedings of the Institution of Mechanical Engineers 171(1) (1957) 669–690.

[10] Torii, T., Yasuda, K., Nonlinear oscillation of a rotating disk subject to a transverse load at a space-fixed point, Proceedings of the X. World Congress on the Theory of Machine and Mechanisms, Oulu, Finland, 1999, pp. 1 752–1 757.

[11] Yan, L.-T., Li, Q.-H., Investigation of travelling wave vibration for bladed disk in turbomachinery, Proceedings of the 3$^{\mathrm{rd}}$ International Conference on Rotordynamics – IFToMM, Lyon, France, 1990, pp. 133–135.